C. R. Chimie 16 (2013) 778–788

Contents lists available at SciVerse ScienceDirect

Comptes Rendus Chimie

www.sciencedirect.com

Full paper/Mémoire

PbTe nanostructures: Microwave-assisted synthesis by using lead Schiff-base precursor, characterization and formation mechanism

Shahla Ahmadian-Fard-Fini [a], Masoud Salavati-Niasari [b,c,*], Azam Monfared [a], Fatemeh Mohandes [b]

[a] Department of Chemistry, Payame Noor University, P. O. Box. 19395-3697 Tehran, Iran
[b] Department of Inorganic Chemistry, Faculty of Chemistry, University of Kashan, P. O. Box. 87317-51167 Kashan, Iran
[c] Institute of Nano Science and Nano Technology, University of Kashan, P. O. Box. 87317-51167 Kashan, Iran

ARTICLE INFO

Article history:
Received 9 January 2013
Accepted after revision 28 March 2013
Available online 9 May 2013

Keywords:
Nanostructures
Semiconductor
Chalcogenide
Nanoparticle
Lead telluride

ABSTRACT

Pure cubic phase lead telluride (PbTe) nanostructures have been produced by using a Schiff-base complex as a precursor in the presence of microwave irradiation. The Schiff base used as ligand was derived from salicylaldehyde and ethylenediamine. The Schiff-base complex was marked as [Pb(salen)]. In addition, the effect of the irradiation time and the type of reducing agent on the morphology and purity of the final products was investigated. The as-synthesized PbTe nanostructures were characterized extensively by techniques like X-ray powder diffraction (XRD), transmission electron microscopy (TEM), and scanning electron microscopy (SEM). The microwave formation mechanism of the PbTe nanostructures was studied by XRD patterns of the products. Although it was found that both ionic and atomic mechanisms could take place for the preparation of PbTe, the main steps were according to the atomic reaction process, which could occur between elemental Pb and Te.

1. Introduction

In the past decades, nano-sized semiconductors have attracted significant attention due to their size-tunable optical properties, which result from three-dimensional quantum confinement [1]. Therefore, it is essential to produce and study materials existing in the limit of strong-quantum confinement. Compared with many traditional II–VI and III–V semiconductors, the IV–VI lead chalcogenide nanostructures have smaller band-gaps and larger Bohr radius. Lead telluride (PbTe) as a member of the chalcogenide family has been widely applied in many fields, such as infrared detectors, photo-resistances, lasers, and thermoelectric materials, because of its small band-gap (0.31 eV at 300 K) and larger Bohr excitation radius (46 nm) [2–6]. Up to now, various methods have been explored to synthesize lead telluride nanostructures, such as room-temperature synthesis process in an alkaline aqueous solution [7,8], electrochemical deposition without any template [9], sonochemical [10,11], pulsed laser fragmentation of PbTe microstructures [12], and alkaline reducing chemical route [13].

In this investigation, PbTe nanostructures have been fabricated by a microwave-assisted method. The use of microwave energy to heat chemical reactions has attracted a considerable amount of attention due to its many advantages, like application in chemistry, material sciences, nanotechnology, and biochemical processes [14–20]. There are many advantages in the microwave-assisted approaches, such as very short reaction times, fast heat transformation, avoidance of local overheating, and controllable reaction temperature. Although Palchik et al. [21], Cao et al. [22], and Kerner et al. [23] have synthesized PbTe nanostructures in the presence of microwave

* Corresponding author.
E-mail address: salavati@kashanu.ac.ir (M. Salavati-Niasari).

1631-0748/$ – see front matter © 2013 Académie des sciences. Published by Elsevier Masson SAS. All rights reserved.
http://dx.doi.org/10.1016/j.crci.2013.03.017

irradiation by using lead acetate as Pb source, we applied a Schiff-base complex as a lead precursor.

Today, coordination compounds have been widely used as precursor for the preparation of various nanostructures to control shape and size distribution [24–30]. Although lead oleate as a coordination compound has been applied to the synthesis of PbTe nanocrystals via an injection solution-phase route [31–33], [Pb(salen)] was used as a precursor to fabricate PbTe nanostructures for the first time. In addition, Te powder and propylene glycol (PG) were utilized as a Te source and a solvent, respectively. To go further into the study, the effect of irradiation time and type of reducing agent on the morphology and purity of PbTe was investigated.

2. Experimental

2.1. Materials and physical measurements

$Pb(NO_3)_2$, salicylaldehyde, ethylenediamine, thriethylamine, Te powder, propylene glycol, hydrazine hydrate ($N_2H_4{\cdot}H_2O$), and KBH_4 were purchased from Merck (pro-analysis) and used without further purification. Fourier transform infrared spectra were recorded using KBr pellets on an FT-IR spectrometer (Magna-IR, 550 Nicolet) in the 400–4000 cm^{-1} range. Powder X-ray diffraction (XRD) patterns were collected with a Philips diffractometer using X'PertPro and the monochromatized Cu Kα radiation (λ = 1.54 Å). The microscopic morphology of the products was visualized by a LEO 1455VP scanning electron microscope (SEM). Energy dispersive X-ray spectrometry (EDS) analysis was done by XL30, Philips microscope. Transmission electron microscope (TEM) images were obtained on a JEM-2100 with an accelerating voltage of 60–200 kV equipped with a high-resolution CCD Camera. The ^1H NMR spectrum of the Schiff base *N,N*-bis(salicylidene)-ethylenediamine, H_2salen, was recorded with a Bruker (400 MHz) instrument in $CDCl_3$. The optical properties of the PbTe nanoparticles were studied with a PerkinElmer spectrophotometer.

2.2. Synthesis of the H_2salen ligand and the [Pb(salen)] complex

A typical procedure for the synthesis of H_2salen ligand is as follows: a solution containing 2 mol of ethylenediamine in 50 mL of methanol was added dropwise into a solution involving 4 mol of salicylaldehyde in 50 mL of methanol. The mixture was refluxed under magnetic stirring for 3 h to produce a yellow precipitate. The yellow H_2salen precipitate was filtered and washed with methanol several times, and finally dried at 50 °C in vacuum. The H_2 ligand was analyzed by ^1H NMR and FT-IR. ^1H NMR (400 MHz, $CDCl_3$) data for the H_2salen are as follows: δ: 13.20 (s, 2H, OH); 8.57 (s, 2H, –CH=N–); 6.85–7.38 (m, 8H, aromatic); 4.00 (s, 4H, $–CH_2–N=C$).

A typical procedure for the synthesis of [Pb(salen)] complex is as follows: 2 mmol of $Pb(NO_3)_2$ were dissolved in 50 mL of methanol. A stoichiometric amount of the H_2salen dissolved in an equal volume of methanol and 2 mL of thriethylamine (Et_3N) were added dropwise into the above solution under magnetic stirring. The as-obtained yellow precipitate was filtered, washed several times with methanol and distilled water to remove impurities, and then dried in vacuum at 50 °C for 12 h. The as-produced lead precursor was characterized by FT-IR. The formation reactions of the H_2salen ligand and the [Pb(salen)] complex were shown in Scheme 1.

2.3. Synthesis of pure cubic phase lead telluride nanostructures

In a typical process, 0.5 g of NaOH was dissolved in 50 mL of distilled water. Then, 0.001 mol of Te powder and 3 mL of hydrazine hydrate (100%) were added into the above solution under gentle heating by magnetic stirring. Then, 0.001 mol of the [Pb(salen)] complex dissolved in 30 mL of propylene glycol (PG) was added dropwise into the solution. The reaction flask was held at the center of a microwave system. The exposure time was done at 5, 30, 120 min. After cooling the flask to room temperature, the gray powder was collected by filtering, washed with distilled water and methanol, and finally dried at 50 °C in vacuum. For the sake of comparison, several experiments were carried out with KBH_4 instead of hydrazine hydrate under the same conditions. In this method, the microwave oven worked in the following cycling mode: on for 10 s, off for 10 s. To investigate the effect of microwave power on the morphology of PbTe, two experiments were carried out at 600 W and 900 W. The preparation conditions for the synthesis of PbTe nanostructures were illustrated in Table 1.

3. Results and discussion

3.1. X-ray powder diffraction studies

In order to study the effect of irradiation time on the purity of PbTe nanostructures, the microwave power was kept constant at 750 W and the irradiation time was changed from 30 min to 120 min. Fig. 1a shows the XRD pattern of the product prepared by using hydrazine

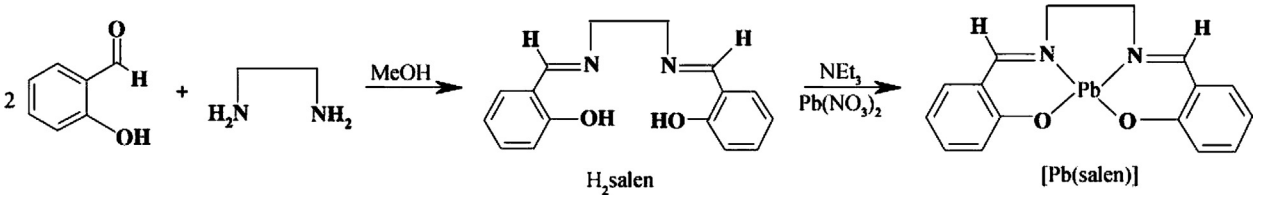

Scheme 1. Chemical reactions for the synthesis of the H_2salen and [Pb(salen)].

Table 1
Preparation conditions of PbTe nanostructures.

Sample no	Lead source	Microwave power (W)	Irradiation time (min)	Reducing agent	Particle size (nm)
1	[Pb(salen)]	750	30	$N_2H_4{\cdot}H_2O$	~25
2	[Pb(salen)]	750	60	$N_2H_4{\cdot}H_2O$	55–60
3	[Pb(salen)]	750	90	$N_2H_4{\cdot}H_2O$	120–150
4	[Pb(salen)]	750	120	$N_2H_4{\cdot}H_2O$	12–15
5	[Pb(salen)]	750	60	KBH_4	15–18
6	[Pb(salen)]	750	90	KBH_4	8–10
7	[Pb(salen)]	750	120	KBH_4	8–12
8	$Pb(NO_3)_2$	750	120	KBH_4	~15
9	[Pb(salen)]	600	60	$N_2H_4{\cdot}H_2O$	90–92
10	[Pb(salen)]	900	60	$N_2{\cdot}H_2O$	95–100
11	$Pb(NO_3)_2$	750	60	$N_2H_4{\cdot}H_2O$	Agglomerated particles

PbTe: pure cubic phase lead telluride.

hydrate as a reductant after irradiation for 30 min (sample 1). The XRD pattern of sample 1 indicated the formation of cubic phase PbTe (space group $Fm\bar{3}m$ JCPDS No. 77-0246). In Fig. 1a, the peaks marked with "○" correspond to the Te powder, indicating the presence of untreated elemental Te with the other reagents. The XRD pattern of the product synthesized after microwave irradiation for 120 min (sample 4) is displayed in Fig. 1b. All of the diffraction peaks in Fig. 1b can be indexed to pure cubic PbTe, with cell constants $a = b = c = 6.4610$ Å (JCPDS card No. 77-0246). These results indicated that the optimum irradiation time to produce pure PbTe was 120 min at 750 W. Besides hydrazine hydrate, the experiment was done by KBH_4 as a reducing agent. Fig. 1c shows the XRD pattern of the product produced at 750 W after irradiation for 120 min in the presence of KBH4 (sample 7). All of the diffraction peaks in Fig. 1c can be attributed to pure cubic PbTe (JCPDS card No. 77-0246). Therefore, by using hydrazine hydrate and KBH_4 after irradiation for 120 min at 750 W, pure PbTe nanostructures have been obtained. To investigate the effect of lead precursor on the formation of PbTe nanostructures, one experiment was performed by using $Pb(NO_3)_2$ salt instead of the [Pb(salen)] complex. The XRD pattern of the product synthesized by $Pb(NO_3)_2$ in the presence of KBH_4 as a reductant after irradiation for 120 min at 750 W (sample 8) is shown on Fig. 1d. The XRD pattern of sample 8 indicated the formation of PbTe along with $Na_2(BO_2(OH))$. In the XRD pattern of sample 8 synthesized with $Pb(NO_3)_2$ (Fig. 1d), the presence of elemental untreated Te was observed. According to the XRD results, it was found that pure PbTe could be obtained by using the [Pb(salen)] complex as a precursor after irradiation for 120 min at 750 W. The crystalline size of the as-synthesized PbTe (Dc) was calculated from the major diffraction peak in the XRD pattern (200) using the Debye–Scherrer formula (Equation 1) [34].

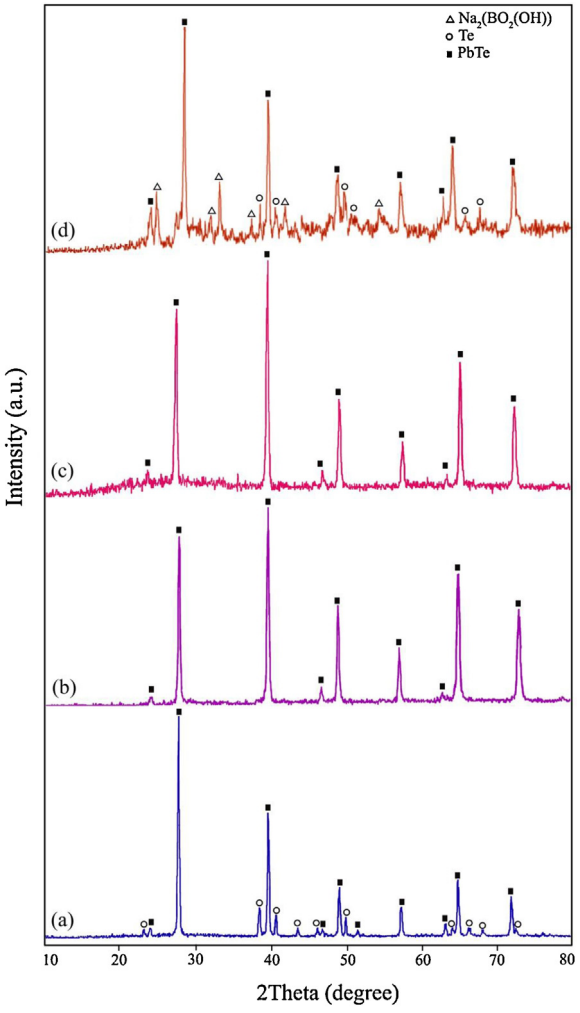

Fig. 1. X-ray powder diffraction patterns of (a) sample 1, (b) sample 4, (c) sample 7, and (d) sample 8.

$$D_c = K\lambda/\beta\cos\theta \quad (1)$$

where K is a constant (0.9); λ is the X-ray wavelength used in XRD (1.5418 Å); θ is the Bragg angle; β is the pure diffraction broadening of a peak at half-height, that is the broadening due to the crystalline dimensions. The crystal diameters of samples 1, 4, 7, and 8 calculated by the Debye–Scherrer formula were about 25, 12, 10, 15 nm, respectively. The XRD results indicated that by using the [Pb(salen)] complex as a precursor at 750 W in the presence of $N_2H_4{\cdot}H_2O$ and KBH_4 as a reducing agent, pure PbTe nanostructures could be produced after microwave irradiation for 120 min.

3.2. Scanning electron microscopy and transmission electron microscopy images

To study the effect of irradiation time on the morphology of the products, SEM images of samples 2–4 produced by $N_2H_4{\cdot}H_2O$ as a reducing agent were taken and presented in Figs. 2a–c, respectively. Fig. 2a shows a SEM image of the product synthesized at 750 W after irradiation for 60 min (sample 2). As shown in Fig. 2a, morphology and particle size of sample 2 are irregular. The morphology of sample 2 is composed of particle-like and rod-like micro/nanostructures. By increasing the irradiation time from 60 min to 90 min (sample 3), only the presence of micro-sized particles was observed (Fig. 2b). When the irradiation time was 120 min (sample 4), PbTe nanoparticles with grain size in the 12–15-nm range were produced (Fig. 2c). In addition, the effect of irradiation time on the morphology of PbTe synthesized by KBH_4 as a reductant was investigated by SEM images. Fig. 3a shows SEM image of

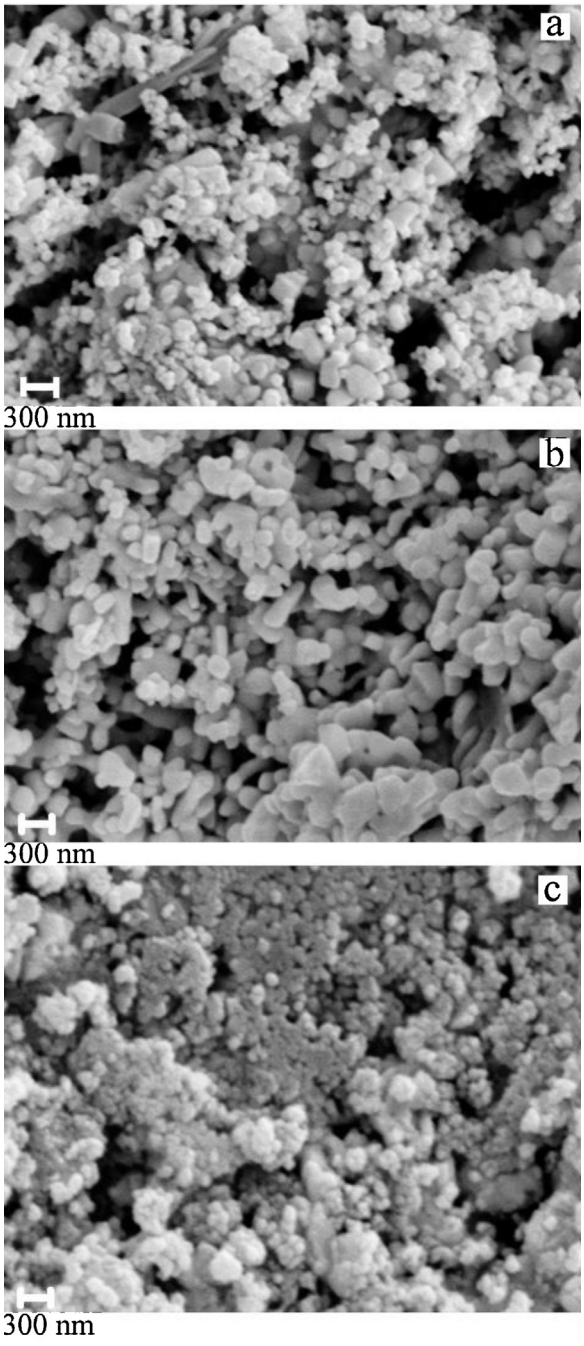

Fig. 2. Scanning electron microscopy images of (a) sample 2, (b) sample 3, and (c) sample 4.

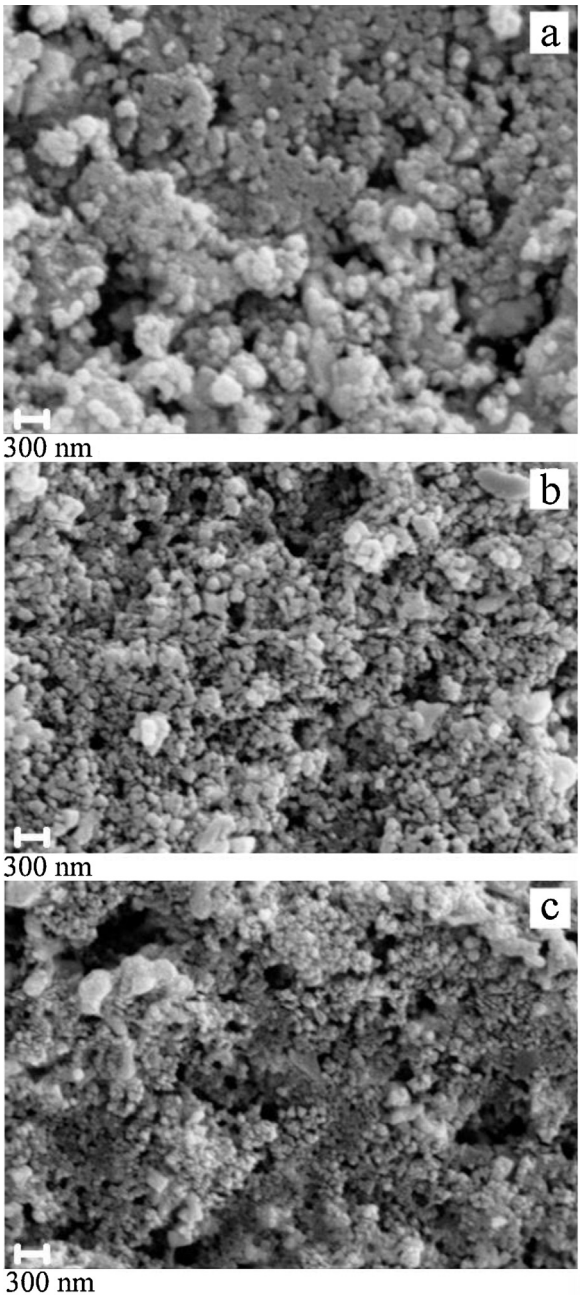

Fig. 3. Scanning electron microscopy images of (a) sample 5, (b) sample 6, and (c) sample 7.

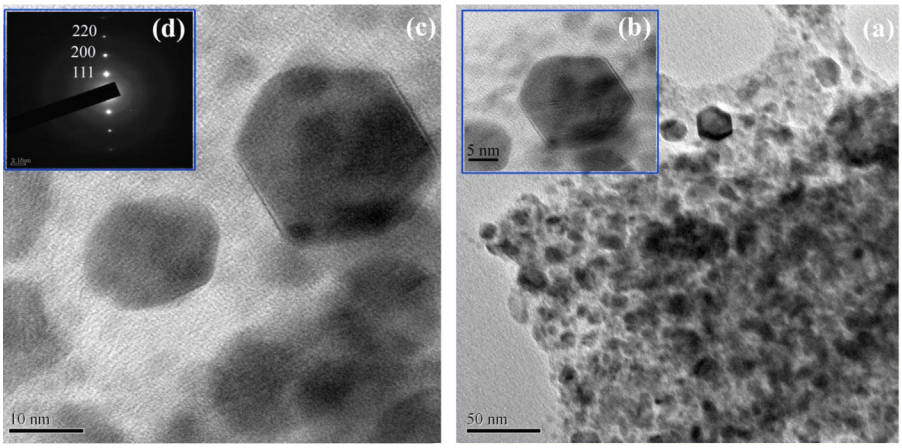

Fig. 4. (a–c) Transmission electron microscopy images and (d) SAED pattern of PbTe nanostructures obtained from sample 4. The rings are characteristic of well-crystallized polycrystals.

the product generated by KBH_4 after irradiation for 60 min (sample 5). In Fig. 3a, it can be seen that the morphology of sample 5 is that of particle-like structures, with a particle size between 15 and 18 nm. Fig. 3b presents the SEM image of the product fabricated by KBH_4 after microwave irradiation for 90 min (sample 6). According to the SEM image displayed in Fig. 3b, the grain size of PbTe nanoparticles from sample 6 is between 8 and 10 nm.

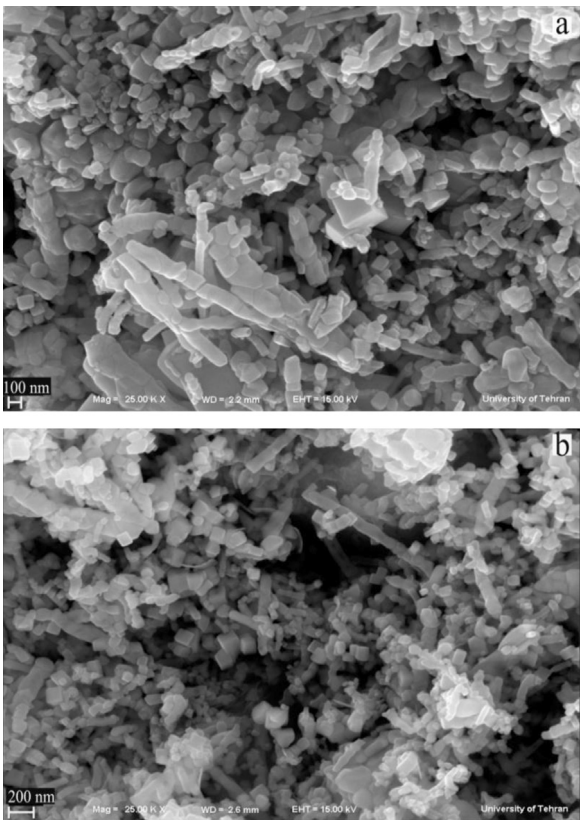

Fig. 5. Scanning electron microscopy images of the products synthesized at 600 W (a) and 900 W (b).

When microwave irradiation was 120 min in the same conditions, PbTe nanoparticles with a particle size about 8–12 nm were formed (Fig. 3c). To further investigate the morphological details, TEM images were taken and shown in Fig. 4. Panels a, b, and c of Fig. 4 are TEM images of sample 4 prepared by $N_2H_4{\cdot}H_2O$ as a reducing agent after irradiation for 120 min. It is possible to detect particle-like and hexahedron PbTe nanostructures in these images. A closer observation of the morphology of sample 4 (Fig. 4c) reveals that the particle size of the PbTe nanostructures is between 10 and 15 nm. These nanostructures are well-crystallized, as it can be observed from the selected area electron diffraction pattern displayed in Fig. 4d. After all, it was concluded that by increasing the irradiation time from 60 to 120 min by using KBH_4 instead of $H_2H_4{\cdot}H_2O$, the particle size of the PbTe nanostructures decreased.

The effect of microwave power on the morphology of PbTe nanostructures prepared by using a microwave-assisted aqueous solution method has been studied. Figs. 5a and 5b show SEM images of the products synthesized at 600 W (sample 9) and 900 W (sample 10) after irradiation for 60 min, respectively. According to these images, it was found that the morphology of samples 9 and 10 synthesized at 600 and 900 W is composed of cubic-like and rod-like nanostructures. In fact, morphology of PbTe nanostructures shifted to nanocubes and nanorods with decreasing and increasing microwave power from 750 W.

3.3. FT-IR spectra

Fig. 6 shows FT-IR spectra of the as-synthesized samples in the range of 400–4000 cm^{-1} range. The FT-IR spectrum of the H_2salen ligand is shown on Fig. 6a. The strong peak at 1632 cm^{-1} is attributed to ν(C=N) as a characteristic band for the Schiff-base ligand. Fig. 6b shows the FT-IR spectrum of the [Pb(salen)] complex. In Fig. 6b, the strong band at 1628 cm^{-1} is assigned to ν(C=N). The ring skeletal vibrations (C=C) of Schiff-base ligand were observed in the region between 1439 and 1533 cm^{-1}. The phenolic C–O stretching vibration is seen at 1277 cm^{-1} in

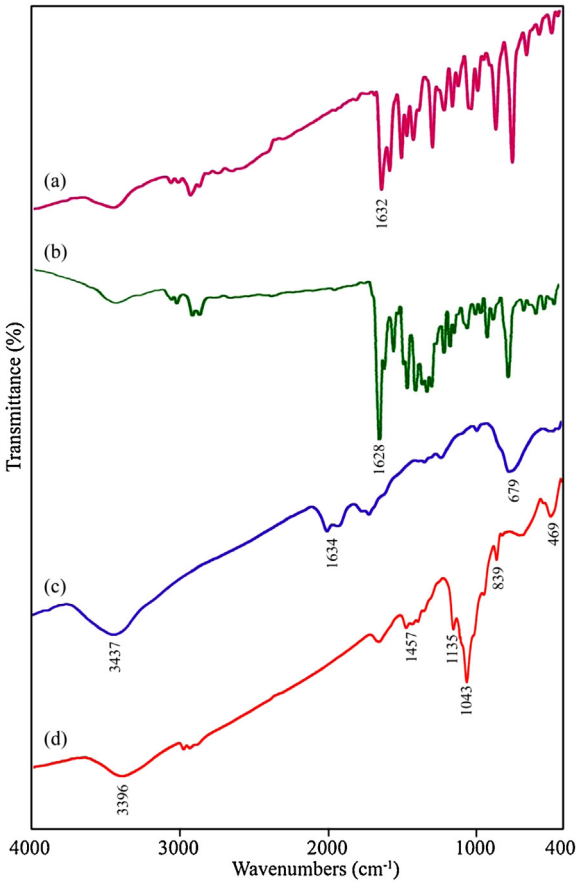

Fig. 6. FT-IR spectra of (a) H_2salen ligand, (b) [Pb(salen)] precursor, PbTe nanostructures obtained from samples 4 (c) and 7 (d).

the FT-IR spectrum of the Schiff-base ligand [35]. The FT-IR spectrum of the [Pb(salen)] complex presented on Fig. 6b showed evidence of the synthesis of the complex, since the bands centered at 1630 cm^{-1} (attributed to $\nu_{C=N}$), 1533 cm^{-1} (attributed to $\nu_{C=C}$) and 1277 cm^{-1} (attributed to ν phenolic C–O) are characteristic peaks of the [Pb(salen)] complex. By comparing the frequency attributed to the ν(C=N) in the IR spectrum of the H_2salen (Fig. 6a) and [Pb(salen)] (Fig. 6b), it was found that this band shifted to lower frequency and appeared at 1628 cm^{-1} in the IR spectrum of the [Pb(salen)], indicating the coordination of the nitrogen atom in the C=N group to the Pb ion. Figs. 6c and 6d show the FT-IR spectra of the PbTe nanoparticles obtained from samples 4 and 7, respectively. In Fig. 6c, the broad absorption band centered at 3437 cm^{-1} and the weak peaks at 1634 and 679 cm^{-1} are attributable to the ν(OH) stretching and bending vibrations, respectively, which indicates the presence of physisorbed water molecules linked to the PbTe nanoparticles [36]. The presence of a broad peak at 3396 cm^{-1} in Fig. 6d is attributed to the ν(OH) stretching vibration. The observation of some weak bands located at 1457, 1135, 1043, 839 and 469 cm^{-1} could be attributable to the absorptions of water and CO_2 molecules from the atmosphere [37]. No characteristic peaks of impurities were observed in the FT-IR spectrum of the PbTe nanostructures.

3.4. Energy dispersive X-ray spectrometry patterns

Figs. 7a and 7b show EDS patterns of the PbTe nanoparticles obtained from samples 4 and 7, respectively. The EDS patterns in Fig. 7 indicate that the elements in samples 4 and 7 are Pb and Te only (Si, and C signals are from the substrate). The EDS results gave a rough atomic Pb:Te ratio close to 1:1, confirming the purity of the nanoparticles.

3.5. Optical property of pure cubic phase lead telluride nanoparticles

The UV–vis spectrum of the PbTe nanoparticles dispersed in ethanol was recorded using a quartz cell (1-cm path length). Fig. 8a depicts the UV–vis spectrum of the PbTe nanoparticles with a particle size between 10 and 15 nm (sample 4). This spectrum shows a strong absorption peak in the visible region. For the PbTe nanoparticles, the absorption peak shifted to 694 nm, which is higher than that of PbTe nanorods synthesized by Sridharan et al. [38]. Fig. 8b shows the plot of $(\alpha h\upsilon)^2$ versus photon energy ($h\upsilon$) for the PbTe nanoparticles. The band-gap value (E_g) of sample 4 was calculated by extending the linear part of the curve to zero absorption. The band-gap estimated of the PbTe nanoparticles was about 1.2 eV. By comparing the band-gap value of the PbTe nanoparticles with band-gap values of PbTe microstructures [9] and hierarchical microcrystals [39], it was found that the band-gap value of the PbTe nanoparticles synthesized according to this method has a blue shift. This blue shift can be related to the small crystallite size of the PbTe nanoparticles (10–15 nm), which leads to a quantum confinement effect [40]. The large excitonic Bohr radius of about 46 nm in PbTe allows a strong-quantum confinement within a large range of particle sizes.

3.6. The formation mechanism of pure cubic phase lead telluride nanostructures

In this work, a Schiff-base complex was synthesized, characterized, and then used as a lead precursor to fabricate PbTe nanostructures. When the [Pb(salen)] molecules were dissolved in propylene glycol, Pb^{2+} ions capped by $salen^{2-}$ were released. In fact, the Schiff-base molecules were applied as surfactants due to their steric hindrance effect. By adding the solution including the Te source to the [Pb(salen)] solution, PbTe nuclei were formed in the presence of microwave irradiation. It was found that PbTe can be formed by two independent pathways, involving ionic and atomic processes. In the ionic process, Pb^{2+} ions react with Te^{2-} ions to generate PbTe nuclei. Besides, a directly atomic process can proceed between elemental Te and Pb. It must be remembered that the Pb^{2+} ions released from the lead precursor can be reduced by $N_2H_4{\cdot}H_2O$ and KBH_4 [41–43]. The formation mechanism of PbTe through both ionic and atomic processes results from redox reactions. According to the standard redox potential

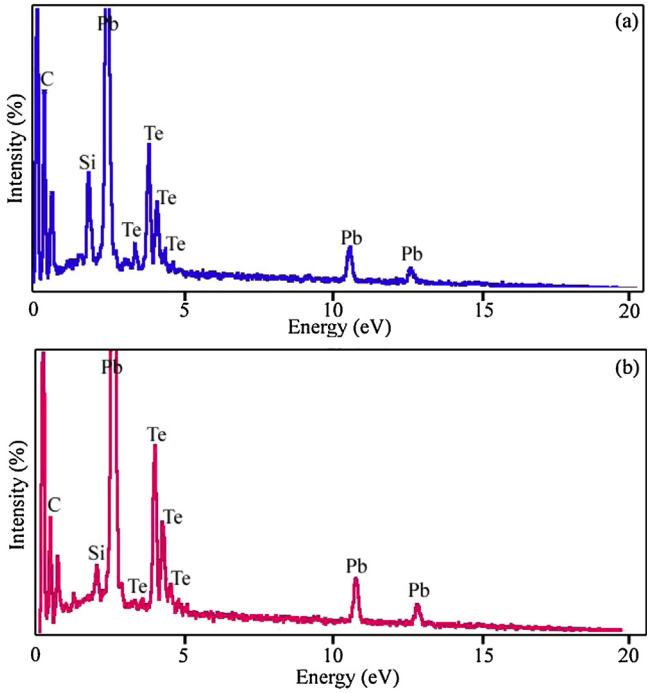

Fig. 7. Energy dispersive X-ray spectrometry spectra of samples 4 (a) and 7 (b).

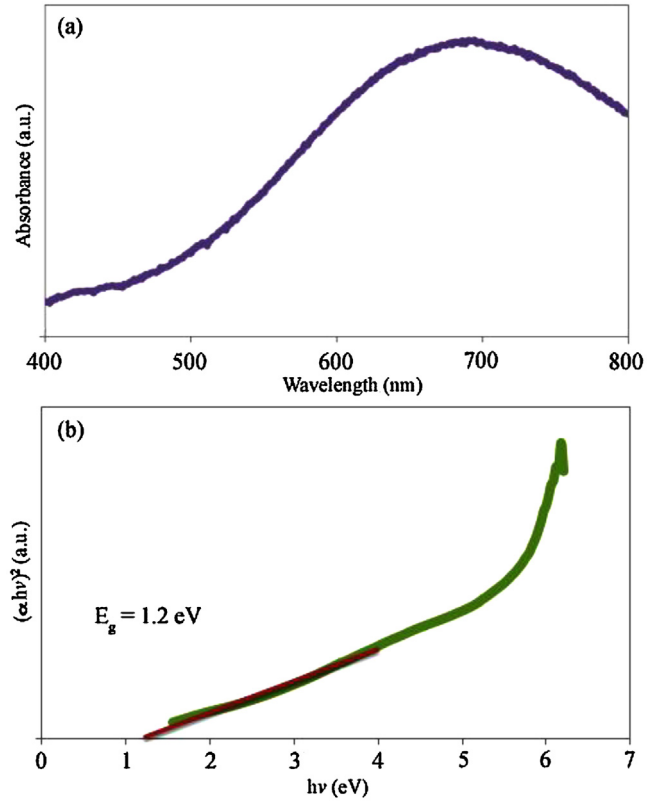

Fig. 8. (a) UV–vis spectrum and (b) the plot of $(\alpha h\nu)^2$ versus $h\nu$ for sample 4.

of Te/Te^{2-} (−1.143 V) and N_2/N_2H_4 (−1.15 V), the Te powder cannot be efficiently reduced to Te^{2-} ions by hydrazine hydrate because of the close redox potentials of Te and N_2H_4. On the other hand, Pb^{2+} ions can be easily reduced by hydrazine hydrate ($E^0_{Pb^{2+}/Pb} = -0.126$ V). To study the formation mechanism of the PbTe nanostructures, four blank tests were done under microwave irradiation at 750 W for 1 h in PG as a solvent. One experiment (blank test No. 1) was carried out with the aid of [Pb(salen)], hydrazine hydrate and NaOH without using Te powder. The XRD pattern of the blank test No. 1 is shown on Fig. 9a. The XRD pattern shows the presence of elemental Pb in the product. This result proved that the Pb^{2+} ions could be reduced by hydrazine hydrate. Besides elemental Pb, lead oxide, lead hydroxide and carbonate are seen on Fig. 9a due to the presence of NaOH in the solution. In this case, there is a question. Why did not elemental lead exist in the final products synthesized in the presence of Te powder? According to the atomic formation mechanism of PbTe, elemental Pb and Te could react with each other to form PbTe.

During the formation process of PbTe, Te powder quickly dissolved into strong alkaline hydrazine hydrate,

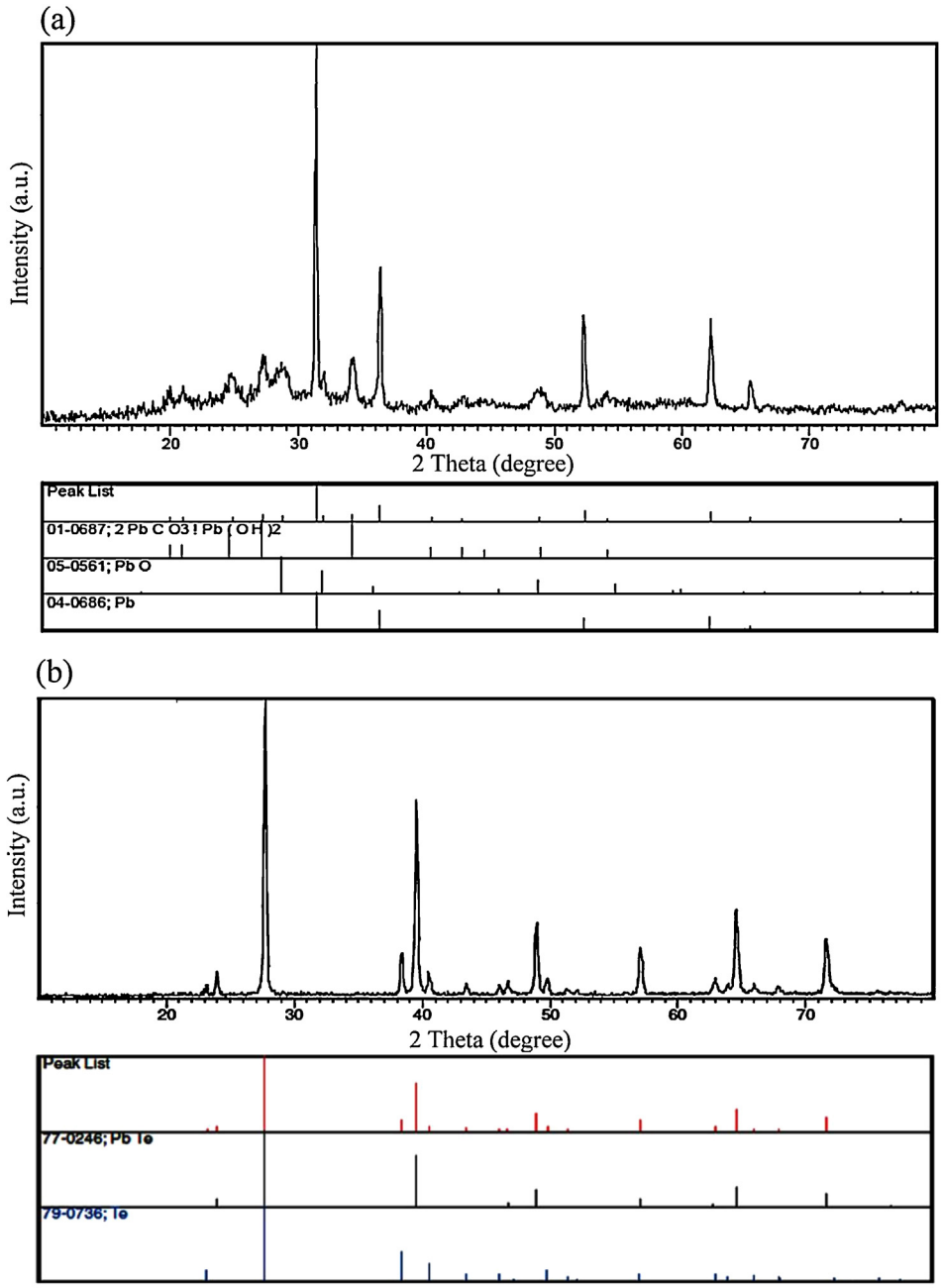

Fig. 9. X-ray powder diffraction patterns of blank tests No. 1 (a) and No. 2 (b).

whereas the color of the solution quickly turned purple black. To study the effect of the alkaline solution on this method, one experiment was done in the absence of NaOH. Fig. 9b shows the XRD pattern of the product obtained without using NaOH (blank test No. 2). As shown in Fig. 9b, the XRD pattern of the product indicates the formation of cubic phase PbTe (space group $Fm\bar{3}m$, JCPDS No. 77-0246) along with hexagonal-phase Te (JCPDS No. 79–0736). Based on this result, we evidenced the presence of Te powder in the solution prepared without NaOH. In fact, the addition of NaOH accelerated the dissolution process of the Te powder. The disproportional reaction of Te can produce TeO_3^{2-} ions, which can reduce to Te_{a+1}^{2-} ions by hydrazine hydrate or KBH_4. Te_{a+1}^{2-} ions with purple black color consist of Te and Te^{2-} ions [41]. To prove the reducing effect of hydrazine hydrate for Te, blank test No. 3 was done in the presence of Te powder, hydrazine hydrate and NaOH, without using lead precursor. The presence of NaH as a by-product in the XRD pattern of the blank test No. 3 (Fig. 10a) indicated that hydrazine hydrate molecules

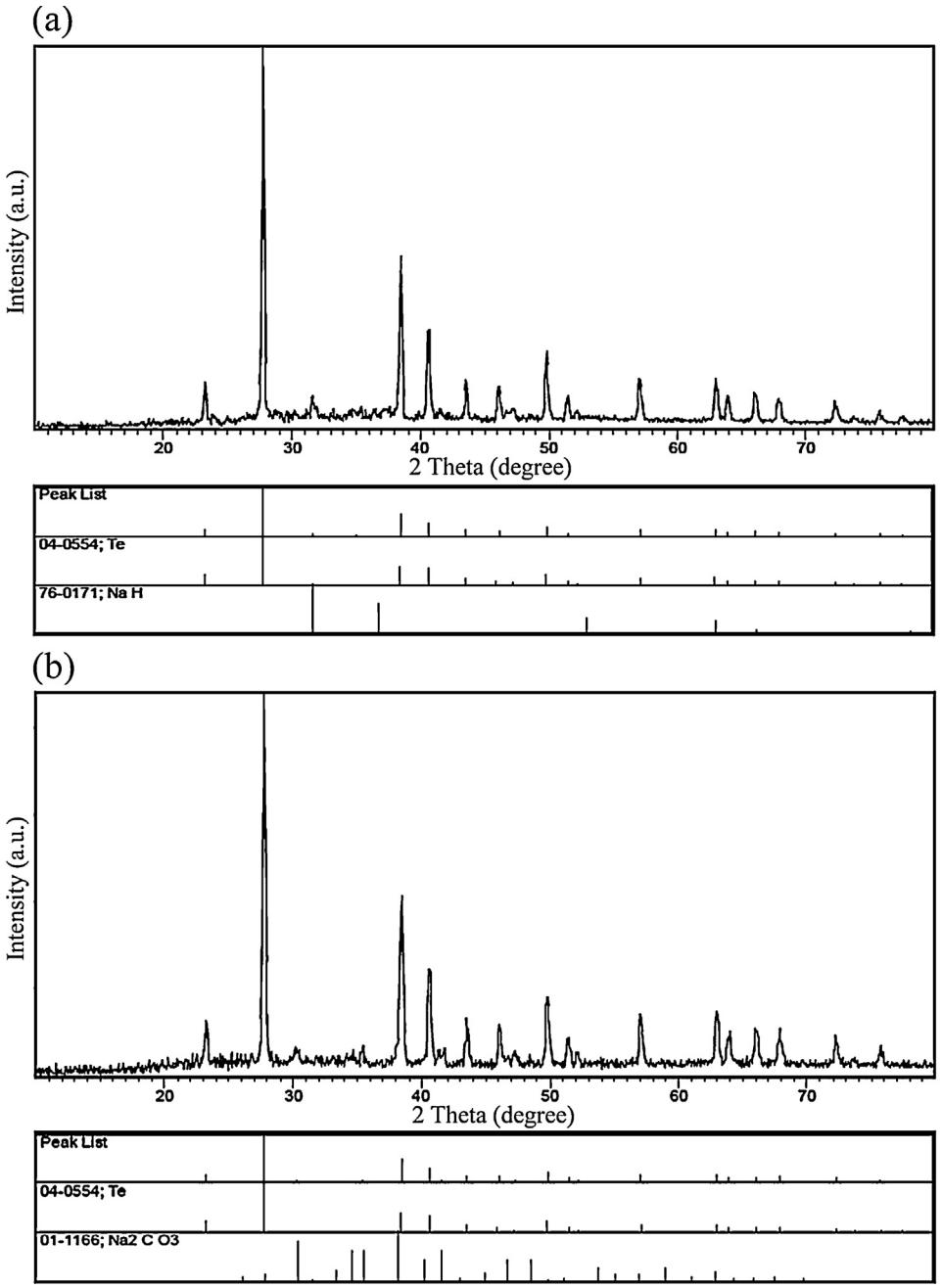

Fig. 10. X-ray powder diffraction patterns of blank tests No. 3 (a) and No. 4 (b).

Table 2
Preparation conditions and corresponding products of blank tests Nos. 1–4.

Blank test no.	[Pb(salen)]	Te powder	$N_2H_4.H_2O$	NaOH	Products	Figure no.
1	Yes	No	Yes	Yes	Pb, PbO, $PbCO_3$, $Pb(OH)_2$	9a
2	Yes	Yes	Yes	No	Te, PbTe	9b
3	No	Yes	Yes	Yes	Te, NaH	10a
4	H_2salen	Yes	Yes	Yes	Te, Na_2CO_3	10b

could release hydride ions to reduce Te powder. In this work, [Pb(salen)] was applied as a lead precursor. The [Pb(salen)] precursor could release Pb^{2+} ions after dissolving in propylene glycol. To find what happened to the *N,N*-bis(salicylidene)-ethylenediamine ligand during the microwave treatment, the experiment was carried out with H_2salen, $N_2H_4{\cdot}H_2O$, NaOH, Te powder under microwave irradiation. This experiment's product was marked as blank test No. 4. The XRD pattern of blank test No. 4 can be seen in Fig. 10b. According to this pattern, it was found that the H_2salen ligand decomposed to carbonate and other gases like H_2O and CO_2 under microwave irradiation. The XRD results of the blank tests were illustrated in Table 2. Based on the XRD results and experimental observations, the main steps for the formation of the PbTe nanostructures with the aid of $N_2H_4{\cdot}H_2O$ are as follows:

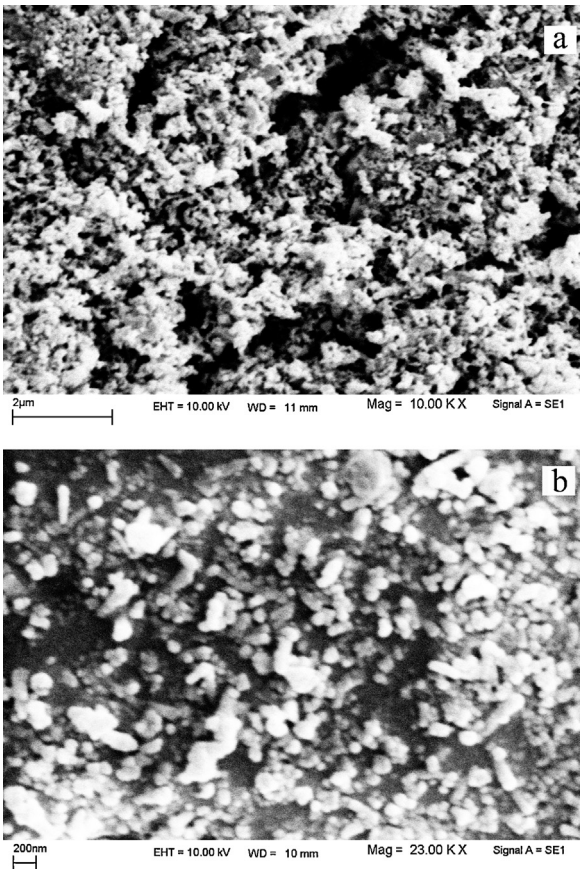

Fig. 11. (a, b) scanning electron microscopy images of the product synthesized with $Pb(NO_3)_2$.

$$3Te + 6OH^- \rightarrow 2Te^{2-} + TeO_3^{2-} + 3H_2O$$
$$TeO_3^{2-} + N_2H_4 + 4OH^- \rightarrow Te_{a+1}^{2-} + N_2 + 4H_2O$$
$$Te_{a+1}^{2-} \rightarrow Te + Te^{2-}$$
$$N_2H_4 + 4OH^- + 2Pb^{2+} \rightarrow 2Pb + N_2 + 4H_2O$$
$$Pb^{2+} + Te^{2-} \rightarrow PbTe$$
$$Pb + Te \rightarrow PbTe$$

When KBH_4 was used instead of $N_2H_4{\cdot}H_2O$, the main reactions were as follows:

$$3Te + 6OH^- \rightarrow 2Te^{2-} + TeO_3^{2-} + 3H_2O$$
$$TeO_3^{2-} + BH_4^- \rightarrow Te + H_2BO_3^- + H_2$$
$$2BH_4^- + 6OH^- + 3Pb^{2+} \rightarrow 3Pb + 2H_2BO_3^- + 5H_2$$
$$Pb^{2+} + Te^{2-} \rightarrow PbTe$$
$$Pb + Te \rightarrow PbTe$$

Therefore, both atomic and ionic processes could take place in the formation mechanism and growth of the PbTe nanostructures.

3.7. Influence of lead precursor on the morphology of pure cubic phase lead telluride

To investigate the effect of the lead precursor on the morphology of PbTe, $Pb(NO_3)_2$ was used instead of the Schiff-base complex in the same conditions. Although in this experiment the preparation conditions (sample 11) were alike those used to synthesize sample 2 in Table 1, $Pb(NO_3)_2$ was used instead of the [Pb(salen)] complex. SEM images of sample 11 with different magnifications are given in Figs. 11a and 11b. Based on the SEM images presented in Fig. 11, it can be seen that PbTe nanoparticles with high agglomeration have been obtained by using $Pb(NO_3)_2$. The particles are highly agglomerated, and it is difficult to measure the individual particle size. By comparing the SEM images of samples 2 (Fig. 2a) and 11 (Fig. 11), it was found that the Schiff-base complex could protect the PbTe nanoparticles from agglomeration due to its steric hindrance effect. In fact, the Schiff-base molecules could act as surfactant in the solution.

4. Conclusion

In summary, PbTe nanostructures have been synthesized with the aid of a Schiff-base complex, Te powder and a reducing agent through a microwave-assisted route. The effects of $N_2H_4{\cdot}H_2O$ and KBH_4 (as reducing agents), of the microwave power and of the irradiation time on the morphology and purity of the PbTe nanostructures were studied. According to SEM micrographs, it was found that KBH_4 as a reducing agent plays a key role in controlling the

nucleation and growth of the PbTe nanoparticles. Based on the XRD results, the optimized irradiation time to prepare pure PbTe nanostructures was 120 min. The XRD results of the blank tests showed that the atomic and ionic processes could occur for the production of PbTe under microwave irradiation.

Acknowledgements

The authors are grateful to the council of the Iran National Science Foundation, University of Kashan, for supporting this work through Grant No. 159271/20, and TEM section, SAIF, NEHU, Shillong, Meghalaya, India, for providing financial support to undertake it.

References

[1] J. Zhu, H. Wang, S. Xu, H. Chen, Langmuir 18 (2002) 3306.
[2] P.S. Nair, K.P. Friz, G. Scholes, Chem. Commun. 24 (2004) 2084.
[3] H. Du, C. Chen, R. Krishan, T.D. Krauss, J.M. Harbold, F.W. Wise, M.G. Thomas, J. Silcox, Nano Lett. 2 (2002) 1321.
[4] H. Zogg, K. Kellermann, K. Alchalabi, D. Zimin, Infrared Phys. Technol. 46 (2004) 155.
[5] V.V. Shchennikov, S.V. Ovsyannikov, Solid State Commun. 126 (2003) 373.
[6] T.C. Harman, R.E. Reeder, M.P. Walsh, B.E. LaForge, C.D. Hoyt, G.W. Turner, Appl. Phys. Lett. 88 (2006) 243504.
[7] Y.Y. Wang, K.F. Cai, X. Yao, J. Solid State Chem. 182 (2009) 3383.
[8] B. Wan, C. Hu, Y. Xi, J. Xu, X. He, Solid State Sci. 12 (2010) 123.
[9] G.R. Li, C.Z. Yao, X.H. Lu, F.L. Zheng, Z.P. Feng, X.L. Yu, C.Y. Su, Y.X. Tong, Chem. Mater. 20 (2008) 3306.
[10] X. Qiu, Y. Lou, A.C.S. Samia, A. Devadoss, J.D. Burgess, S. Dayal, C. Burda, Angew. Chem. 117 (2005) 6005.
[11] Q. Li, Y. Ding, M. Shao, J. Wu, G. Yu, Y. Qian, Mater. Res. Bull. 38 (2003) 539.
[12] C. Chubilleau, B. Lenoir, S. Migot, A. Dauscher, J. Colloid Interface Sci. 357 (2011) 13.
[13] X. Chen, T.J. Zhu, X.B. Zhao, J. Cryst. Growth 311 (2009) 3179.
[14] J.R. Lill, Microwave Assisted Proteomics, RSC Publishing, Cambridge, 2009.
[15] D. Bogdal, A. Prociak, Microwave-Enhanced Polymer Chemistry and Technology, Blackwell Publishing, Oxford, 2007.
[16] N. Mir, M. Salavati-Niasari, F. Davar, Chem. Eng. J. 181–182 (2012) 779.
[17] M. Salavati-Niasari, M. Ranjbar, F. Mohandes, Micro Nano Lett. 7 (2012) 581.
[18] M. Ranjbar, M. Salavati-Niasari, S.M. Hosseinpour-Mashkani, J. Inorg. Organomet. Polym. Mater. 22 (2012) 1093.
[19] M. Sabet, M. Salavati-Niasari, F. Davar, Micro Nano Lett. 6 (2011) 904.
[20] M. Yousefi, M. Sabet, M. Salavati-Niasari, S.M. Hosseinpour-Mashkani, J. Clust. Sci. 23 (2012) 491.
[21] O. Palchik, R. Kerner, A. Gedanken, V. Palchik, M.A. Slifkin, A.M. Weiss, Glass Phys. Chem. 31 (2005) 80.
[22] H. Cao, Q. Gong, X. Qian, H. Wang, J. Zai, Z. Zhu, Cryst. Growth Des. 7 (2007) 425.
[23] R. Kerner, O. Palchik, A. Gedanken, Chem. Mater. 13 (2001) 1413–1419.
[24] F. Mohandes, F. Davar, M. Salavati-Niasari, J. Phys. Chem. Solids 71 (2010) 1623.
[25] M. Salavati-Niasari, F. Mohandes, F. Davar, K. Saberyan, Appl. Surf. Sci. 256 (2009) 1476.
[26] F. Mohandes, F. Davar, M. Salavati-Niasari, J. Magn. Magn. Mater. 322 (2010) 872.
[27] F. Mohandes, F. Davar, M. Salavati-Niasari, Current Nanosci. 7 (2011) 260.
[28] F. Soofivand, F. Mohandes, M. Salavati-Niasari, Micro Nano Lett. 7 (2012) 283.
[29] S.M. Hosseinpour-Mashkani, F. Mohandes, M. Salavati-Niasari, K. Venkateswara-Rao, Mater. Res. Bull. 47 (2012) 3148.
[30] F. Davar, F. Mohandes, M. Salavati-Niasari, Polyhedron 29 (2010) 3132.
[31] Z. Lin, M. Wang, L. Wei, X. Song, Y. Xue, X. Yao, J. Alloys Compd. 509 (2011) 5047.
[32] J.E. Murphy, M.C. Beard, A.G. Norman, S.P. Ahrenkiel, J.C. Johnson, P. Yu, O.I. Mićić, R.J. Ellingson, A.J. Nozik, J. Am. Chem. Soc. 128 (2006) 3241.
[33] J.J. Urban, D.V. Talapin, E.V. Shevchenko, C.B. Murray, J. Am. Chem. Soc. 128 (2006) 3248.
[34] R. Jenkins, R.L. Snyder, Chemical Analysis: Introduction to X-ray Powder Diffractometry, John Wiley and Sons Inc., New York, 1996.
[35] A. Kazemi-Babaheydari, M. Salavti-Niasari, A. Khansari, Particuology 10 (2012) 759.
[36] E. Esmaeili, M. Salavati-Niasari, F. Mohandes, F. Davar, H. Seyghalkar, Chem. Eng. J. 170 (2011) 278.
[37] G. Herrera, E. Chavira, J. Jiménez-Mier, A. Ordoñez, E. Fregoso-Israel, L. Baños, E. Bucio, J. Guzmán, O. Novelo, C. Flores, J. Alloys Compd. 479 (2009) 511.
[38] K. Sridharan, V. Tamilselvan, D. Yuvaraj, K.N. Rao, R. Philip, Opt. Mater. 34 (2012) 639.
[39] T.J. Zhu, X. Chen, Y.Q. Cao, X.B. Zhao, J. Phys. Chem. C 113 (2009) 8085.
[40] S. Gorer, A. Albu-Yaron, G. Hodes, J. Phys. Chem. 99 (1995) 16442.
[41] T.J. Zhu, Y.Q. Liu, X.B. Zhao, Mater. Res. Bull. 43 (2008) 2850.
[42] B. Wan, C. Hu, B. Feng, Y. Xi, X. He, Mater. Sci. Eng., B 163 (2009) 57.
[43] Y.Q. Cao, T.J. Zhu, X.B. Zhao, J. Alloys Compd. 493 (2010) 423.